Journal of Hazardous Materials 475 (2024) 134864

Contents lists available at ScienceDirect

Journal of Hazardous Materials

journal homepage: www.elsevier.com/locate/jhazmat

Machine learning-derived dose-response relationships considering interactions in mixtures: Applications to the oxidative potential of particulate matter

Charles O. Esu [a], JongCheol Pyo [a], Kuk Cho [a,b,*]

[a] Department of Environmental Engineering, Pusan National University, Republic of Korea
[b] Institute of Environmental Studies, Pusan National University, 2 Busandaehak-ro 63beon-gil, Geumjeong-gu, Busan 46241, Republic of Korea

HIGHLIGHTS

- A new ML/explainable AI approach, namely, FLIT-SHAP, was developed.
- It can extract dose-response relationships from multi-pollutant toxicity data.
- It predicted lower OP for real PM samples implying antagonistic interactions.
- It demonstrated higher prediction accuracy than the traditional additive model.
- It emphasized the significance of quinones for OP of PM.

GRAPHICAL ABSTRACT

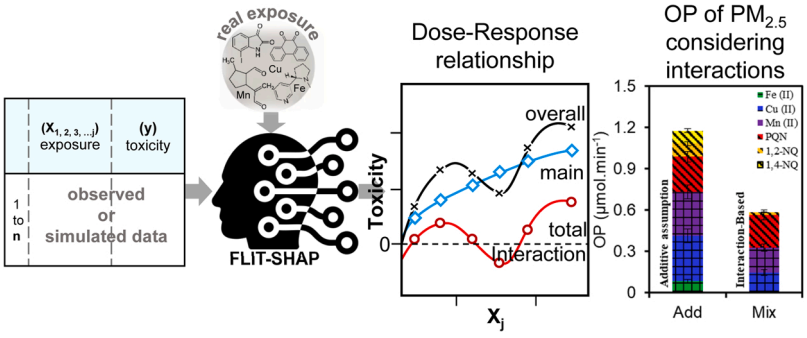

ARTICLE INFO

Keywords:
Chemical exposure
Toxicity
Multi-pollutants
SHAP
PM
OP

ABSTRACT

Conventional environmental health research is primarily focused on isolated chemical exposures, neglecting the complex interactions between multiple pollutants that may synergistically or antagonistically influence toxicity, thereby posing unexpected health risks. In this study, we address this knowledge gap by introducing an explainable machine learning (ML) approach with Feature Localized Intercept Transformed-Shapley Additive Explanations (FLIT-SHAP) designed to extract the dose-response relationships of specific pollutants in mixtures. In contrast to traditional SHAP, FLIT-SHAP can localize the global intercept to elucidate mixture effects, which is crucial for understanding the oxidative potential (OP) of ambient particulate matter (PM). Assessing multi-pollutant OP using FLIT-SHAP revealed both synergistic (55–63 %) and antagonistic (25–42 %) effects in laboratory-controlled OP data, but an antagonistic (33–66 %; lower OP) effect in ambient PM. Notably, the FLIT-SHAP approach demonstrated higher prediction accuracy (R^2 = 0.99) compared to the additive model (R^2 = 0.89) when evaluated against real-world PM samples. Quinones, such as phenanthrenequinone, play a more significant role in $PM_{2.5}$ than previously recognized. Through this study, we highlighted the potential of FLIT-SHAP to enhance toxicity predictions and aid decision-making in the field of environmental health.

* Corresponding author at: Department of Environmental Engineering, Pusan National University, Republic of Korea.
E-mail address: kukcho@pusan.ac.kr (K. Cho).

https://doi.org/10.1016/j.jhazmat.2024.134864
Received 1 February 2024; Received in revised form 3 June 2024; Accepted 7 June 2024
Available online 8 June 2024

1. Introduction

Traditionally, environmental health research is focused on examining the link between exposure to specific chemicals and individual/multi-level biological toxicity [1]. However, real exposure scenarios often involve a combination of pollutants that can synergistically or antagonistically influence each other's toxicity, potentially posing additional health risks than expected [2]. Such multi-pollutant exposures are widespread, including air and soil pollution from incinerators, leaks from hazardous waste sites, and chemical residue in drinking water [3]. Traditional models, such as the concentration addition (CA) and independent action (IA), assume additivity in a mixture for predicting the toxicity of a mixture [4]. This approach is questionable as various cases have shown non-additive toxicity in binary mixtures of pesticides [5], fungicides and insecticides [6], particulate matter (PM) [7], and others [8].

Advanced statistical and machine learning (ML) methods have helped tackle multi-pollutant exposure concerns [9]. Statistical approaches, such as Bayesian kernel machine regression [10], weighted quantile sum regression [11], and quantile g-computation [12], are used to enhance the prediction accuracy of the effects of chemical mixtures. However, additive effects are often assumed in these methods, wherein large numbers of toxic substances and collinearity among variables hinder their efficacy. To overcome these limitations, in recent ML approaches, interactions among multiple environmental chemicals in childhood asthma [13] and autism spectrum disorder [14] have been explored by combining ML and statistical techniques. However, these studies primarily identified combinations of pollutants linked to specific health outcomes, without focusing on dose-response relationships and individual pollutant effects that are crucial for toxicological decision-making [15]. Overall, there is a notable absence of ML-based studies investigating dose-response relationships, while also considering interactions within mixtures.

We addressed this gap by developing an explainable ML approach defined as Feature Localized Intercept Transformed-Shapley Additive Explanations (FLIT-SHAP). Although SHAP can elucidate ML model outputs [16,17], it cannot determine the dose-response curves as it does not predict the absolute response values but relies on a global intercept and the changes for each variable. In contrast, FLIT-SHAP localizes SHAP's global intercept to extract the effect of specific pollutants in mixtures and their dose-response patterns. To explore the applicability of FLIT-SHAP, we examined the oxidative potential (OP) of ambient PM in a multi-pollutant framework. Oxidative stress mediates adverse outcomes driven by environmental chemicals [18], and the OP of whole PM extracts, individual species, and binary interactions have been measured in previous studies [18–38]. In laboratory-controlled, multi-pollutant OP measurements, FLIT-SHAP was used to extract the overall, main, and total-interaction (both synergistic and antagonistic) dose-response relationships for individual pollutants, as learned by the robust eXtreme Gradient Boosting (XGBoost) technique [39]. The predictions of OP of PMs revealed antagonistic effects depending on the species concentrations, highlighting the potential of FLIT-SHAP for more realistic toxicity predictions and better decision-making.

2. Methods

2.1. Data

2.1.1. Laboratory-simulated OP Measurement

To understand the relationship between the concentration and OP, we conducted laboratory-simulated measurements of OP using a mixture of six redox-active species known for their substantial environmental presence and contribution to OP: phenanthrenequinone (PQN), 1,2-naphthoquinone (1,2-NQ), 1,4-naphthoquinone (1,4-NQ), Cu(II), Mn(II), and Fe(II). Although Fe(III) is the dominant iron species in PM, Fe(II) was selected because (1) Fe(II) is more soluble than Fe(III) [40], and (2) Fe(II) has been shown to have approximately three times higher intrinsic OP than Fe(III) [22]. Different combinations of these species were created, resulting in 100 samples. We utilized the dithiothreitol (DTT) assay, a widely adopted method known for its sensitivity to various redox-active metals and quinones, as well as its relevance to health-related outcomes [41,22,42–46,37]. The specifications of all chemicals used and the procedure for stock solution preparation are detailed in the Supplementary Information (**Text S1**). In accordance with previous studies using DTT, we followed the procedure proposed by Li et al. [46], with further modifications made by Lin et al. [47] to ensure robust results (Fig. S1). Briefly, a 100-μL aliquot of the sample (acetonitrile for quinones and DI water for metals) was mixed with 850 μL of phosphate buffer (pH = 7.4, 0.1 M) in a 2-mL polypropylene vial. A 50-μL aliquot of 0.4 mM DTT solution was then added, and the mixture was incubated at 37 °C in a thermomixer. At different time intervals (0, 15, and 30 min), a 100-μL aliquot of 1.0 mM 5,5′-dithiobis (2-nitrobenzoic acid) (DTNB) was added to the reaction solution, and the absorbance (A) of the resulting-colored product was then measured using a UV/Vis spectrophotometer (OPTIZEN POP, KLab, Korea) at 412 nm within 30 min. Finally, the total DTT consumption was determined from the slope of the plot of linear regression of A versus time. PQN was used as a model compound for quality control (QC) of the analysis. For QC, daily DTT consumption was measured for the blank (acetonitrile or DI water + buffer) and 0.25 μM PQN (Fig. S2). The blank-corrected OP of PQN was consistent with that of previous studies [48–50], considering the initial DTT concentration effect observed by Lin et al. [47].

2.1.2. Real samples for prediction

The real ambient PM samples was used, as discussed in **Text S2**. Two types of samples were considered: a hypothetical $PM_{2.5}$ sample (HS) [22] and a size-distributed sample collected during haze/non-haze periods [34]. A summary of the species concentrations in these samples is presented in Table S1.

2.2. Models: Random forest (RF) and XGBoost models

The concentrations of the species and OP of the mixtures were used for training the models. We used an exposure dataset containing j toxic species concentrations or exposure as X with the associated toxicity or health outcome as y for n samples. In our case study of OP, laboratory-simulated OP measurements were employed (previous section). The entire exposure data were randomly split into the training and test sets at a ratio of 75:25. Subsequently, an ML model was trained and evaluated. This process was conducted five times.

RF and XGBoost were applied to predict the OP. These are ensemble learning methods with strong predictive power and robust optimization methods that outperform neural networks on tabular data [16] and are widely applied in air pollution [51,52] and chemical toxicity studies [53]. At the initial stages, we tested both RF and XGBoost; subsequently, we focused on XGBoost as it showed better performance than RF (Table 1). The best model obtained from hyperparameter tuning (training) was then further evaluated using the test data based on the mean absolute error (MAE), root mean square error (RMSE) and coefficient of variation (R^2). Detailed information on the models and parameters can be found in **Text S3**.

Table 1
Summary of the training and validation of the RF and XGBoost models.

metric	75 % Training (1000 bootstraps)		25 % Validation (hold out)	
	RF	XGBoost	RF	XGBoost
R^2	0.97 ± 0.005	0.99 ± 0.0006	0.91	0.93
MAE	0.057 ± 0.005	0.011 ± 0.002	0.081	0.077
RMSE	0.073 ± 0.006	0.019 ± 0.003	0.100	0.091

2.3. Explainable ML: Novel approach using FLIT-SHAP

After developing the robust machine learning model, we established an approach called FLIT-SHAP to extract the dose-response relationships and distinguish the effects of individual pollutants on a health endpoint in multi-chemical mixtures (Fig. 1). FLIT-SHAP is inspired by the SHAP approach for explaining ML models. SHAP is a game-theoretic approach that can achieve a fair distribution of the total toxicity or health endpoint anomaly among different features or species [16,54]. In particular, the contribution of a species or feature (e.g., j among $\mathscr{F}$ features) is determined by comparing model predictions with and without j [17]. This difference was computed for all possible variable subset combinations, considering the interactive effects between variables. Detailed equations can be found in **Text S4**. In general, Eq. 1 is the surrogate model of SHAP.

$$f(x) = E[f(x)] + \sum_{j=1}^{\mathscr{F}} f(\phi_j) \tag{1}$$

The SHAP value (**SV**) of feature j is denoted by $f(\phi_j)$, and it indicates the overall contribution of species j to the endpoint $f(x)$. $E[f(x)]$ is the average value or intercept of the base model prediction for all samples [16,17]. When $\phi_j > 0$ (or $\phi_j < 0$), variable j is known to have a positive (or negative) impact, causing the prediction to increase (or decrease) from the base value.

To calculate the main effect (**ME**) of feature j, denoted as ϕ_{jj}, the interaction effects are subtracted from the SHAP values (Eq. 2). The interaction effect (**IE**) ϕ_{ij} (Equation S4) is the contribution of j in the presence of another feature i, and is summed over all features except j.

$$\phi_{jj} = \phi_j - \sum_{j \neq i} \phi_{ij} \tag{2}$$

The general problem of SHAP values is that they cannot sum to the prediction value without the global intercept value (Eq. 1). This complicates the estimation of the actual intrinsic effect of each feature, which should be summed up to the prediction for that sample. To address this problem, we localized the global intercept value into feature-specific intercept values, $E_j[f(x)]$, using Eq. 3, which was established on the relative importance of each feature. $\langle|\phi_j|\rangle$ is the mean absolute SHAP value for each species. This is the basis of the FLIT-SHAP approach. Therefore, the overall and main effect of a feature can be summed with its localized intercept value to obtain an estimate of its actual overall (SV*) and main (ME*) effects in the sample (Eqs. 4 and 5). The difference between the transformed overall and main effects results

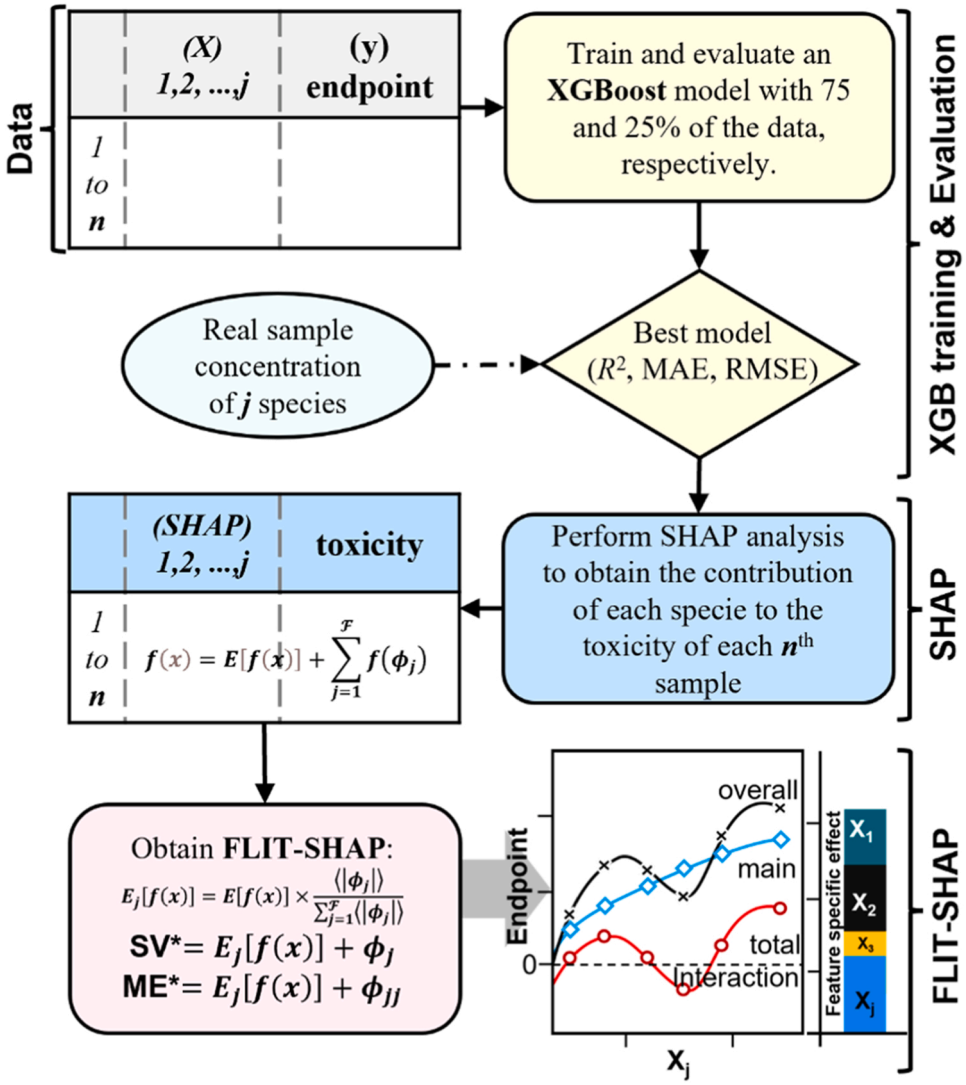

Fig. 1. Study overview. The first stage involves the accumulation of exposure data featuring pollutants (X) and health outcomes (y). The second stage involves the training and evaluation of the XGBoost models. The best model from the second stage is explained in the third stage using SHAP. Finally, FLIT-SHAP is applied to the SHAP results to extract the overall and main effects and the total-interaction dose-response relationships between each X and y to predict the mixture effect of X_j.

in the total interaction effect (Eq. 6), which serves as a check for FLIT-SHAP.

$$E_j[f(x)] = E[f(x)] \times \frac{\langle|\phi_j|\rangle}{\sum_{j=1}^{\mathcal{F}}\langle|\phi_j|\rangle} \tag{3}$$

$$SV* = E_j[f(x)] + \phi_j \tag{4}$$

$$ME* = E_j[f(x)] + \phi_{jj} \tag{5}$$

$$SV* - ME* = IE \tag{6}$$

The following rules are applied: SV* > ME* (synergistic effect, IE > 0), SV* < ME* (antagonistic effect, IE < 0), and SV* ≈ ME* (additive effect, IE ≈ 0). The summation of the IE between feature j and other species i for each sample can be aggregated to form a dose-response relationship for the multi-chemical interaction of j. Similarly, aggregating SV* and ME* for all samples will help determine the overall- and main-effect dose-response relationship for j in a multi-chemical mixture. The performance of FLIT-SHAP explanations was evaluated using standard metrics, with a high R^2 of 0.99, a low RMSE of 0.01 μmol/min, and a low MAE of 0.007 μmol/min, confirming their efficacy (Table S2). The XGBoost model and SHAP package were provided by "scikit-learn" in a Python environment [55].

3. Results

3.1. Model training and evaluation

Effective workflows for ML require representative data. The summary and distribution of the data (concentration and OP) are presented in Table S3 and shown in Fig. S3, respectively. The concentration range for each species was determined based on the environmental concentration range reported in the literature [22; 34]. The minimum concentration was set to zero to mimic situations wherein a species either did not exist or existed at very low concentrations. Furthermore, we confirmed the lack of multicollinearity between the features, as shown in Fig. S4. Using the data, we trained the RF and XGBoost models, and the optimal hyperparameters for the best XGBoost and RF models are presented in Table S4. The performance scores of the RF and XGBoost models with 75 % training sets in 1000 bootstraps and 25 % test sets are summarized in Table 1. XGBoost showed a better performance, wherein the R^2, MAE, and RMSE values were 0.93, 0.077 μmol/min, and 0.091 μmol/min, respectively. Fig. S5 shows the learning curves of XGBoost. These curves indicate that as the number of training samples increased, the accuracy (R^2) of the test set steadily improved until saturation. This suggests that the model acquired sufficient knowledge and may not require larger datasets to enhance its ability to generalize.

3.2. Importance of the species to toxicity

To determine the global importance of features, we used the best model to fit all samples and calculated the SHAP values for each feature in each sample for five separate runs of the steps shown in Fig. 2. The most significant features were identified by determining the average of the absolute SHAP values for each feature over the 100 samples. As shown in Fig. 2**a**, our results demonstrate that globally, PQN is the most important species, whereas Fe is the least important to OP. This is consistent with previous studies stating that the DTT consumption of PQN is the highest, whereas that of Fe is the lowest. The order of importance of quinones and metals (PQN > 1,2-NQ > Cu > 1,4-NQ > Mn > Fe) corresponded to that indicated in a previous study [22]. Moreover, the Gini importance for XGBoost and RF (Fig. S6) showed similar trends. The local information embedded within the global SHAP values is shown in Fig. 2**b**. This visualization depicts all SHAP values for the features using a violin-like scatter plot. We found that the high contribution of the PQN was largely attributed to clusters exhibiting high and low feature values, which accounted for the highest positive and negative marginal contributions to the output of the model, respectively. This suggests that PQN may significantly increase or decrease the overall OP. Similar trends were observed for other species, albeit at lower magnitudes. In general, we observed that increasing the concentration of redox-active species led to an overall increase in the OP.

3.3. Multi-pollutant dose-response relationships using FLIT-SHAP

In previous studies, dose-response relationships for pure species were identified. However, considering that exposures are usually related to multi-pollutant mixtures, one of our objectives was to explore dose-response relationships in a multi-pollutant mixture. The dose-response relationships for the overall (SV*), main (ME*), and total interaction (IE) effects are shown in Fig. 3. The dose-response relationships for quinones were obtained for extended concentration ranges compared to those shown in Table S1, as quinone concentrations can vary across locations. Additionally, the total 1,2-NQ concentration, including both vapor and particle phases, was reported to be 37 times higher than the particle phase concentration alone [56]. The localized intercepts from the FLIT-SHAP analysis are presented in Table S6. The total interaction is the sum of interactions between one species and each of the other (five) species in a sample. The interaction pair and summary plots are shown in Figs. S7 and S8, respectively.

For both the SV* and ME*, high concentrations of redox-active species generally resulted in increased OP, although the magnitude of the SHAP values varied among species. The dominant vertical dispersions observed for SV* indicate different toxicities at the same concentration, implying the complexity of the IE associated with the multi-pollutant mixture. This is the key difference between pure and multi-

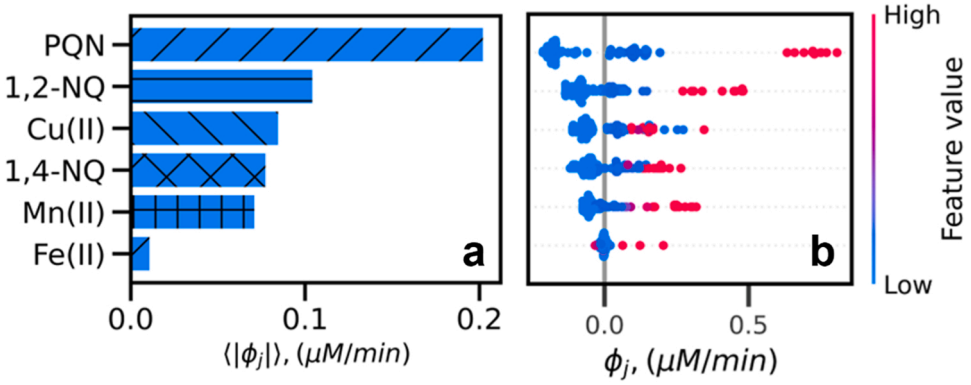

Fig. 2. SHAP feature importance. (a) Species importance to OP. The bars represent the mean value of the absolute SHAP values for each species. The means and standard deviations of five separate runs are presented in Table S5. (b) SHAP values for all samples. The color represents the feature value (i.e., concentration).

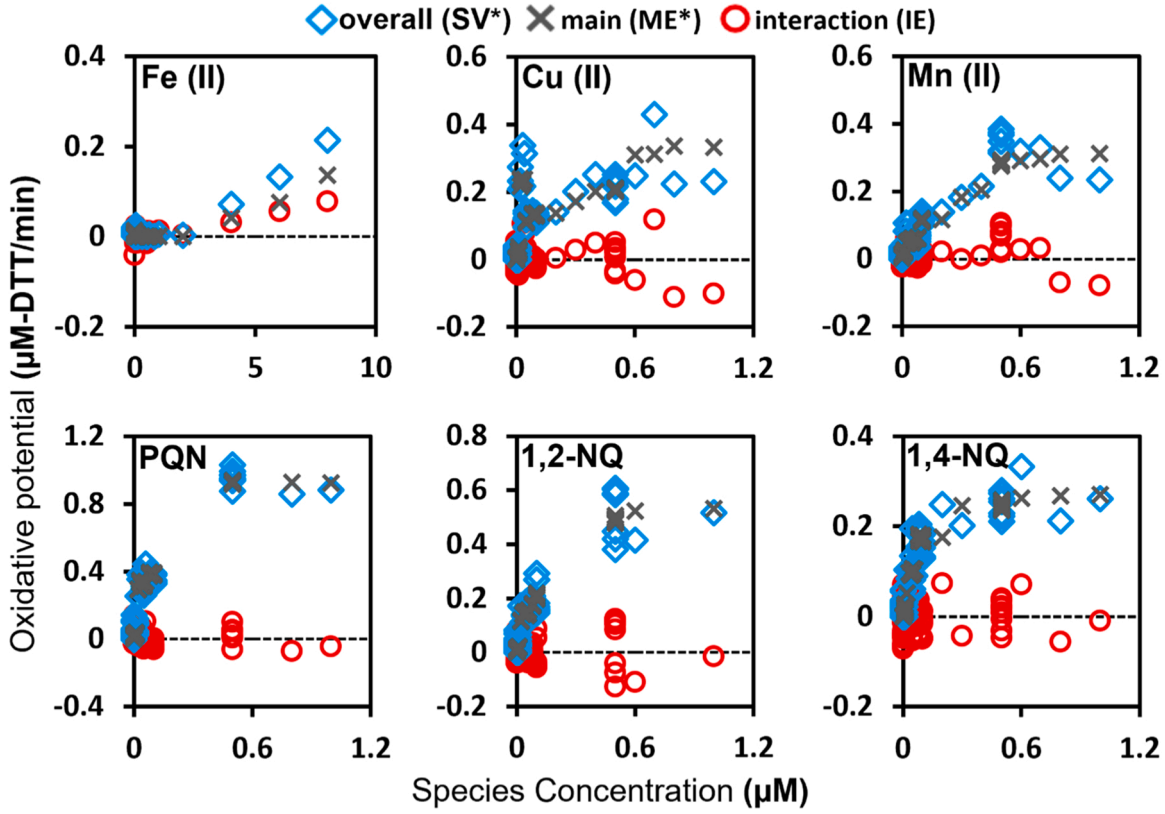

Fig. 3. Multi-pollutant dose-response relationship. The FLIT-SHAP values (SV*), which indicate the overall mixture effect and the corresponding transformed main effect (ME*), plotted against concentrations for the 100 laboratory-simulated samples for each species in the mixture. The total interaction effect (IE) is the sum of the interactions between one species and each of the other species in a mixture. For IE > 0, SV > ME (synergistic); IE < 0, SV < ME (antagonistic); IE ≈ 0, SV ≈ ME (additive). All the values are averages of five separate runs, as shown in Fig. 1. The details of the averages and uncertainties from multiple runs are presented in Tables S7 and S8. In summary, the maximum standard deviation across all effects, species, and samples is ± 0.0031 μmol/min.

pollutant dose-response relationships. The shapes of the ME* dose-response curves generally ranged from linear to nonlinear for all species, excluding Fe. Previous experimental studies for a single species showed a nonlinear OP dose-response relationships for Cu and Mn [22; 34], which corresponds to the results of this study. Although a linear response has been reported for quinones, the trend matched with that in our study considering the concentration ranges. As expected from the importance (Fig. 2), PQN showed the highest OP. The value at a concentration of 0.5 μM was approximately 1.0 μM/min, which matches well with that of previous studies considering the concentration of DTT. Therefore, the OP prediction of the main effect using XGBoost and FLIT-SHAP matched well with that of the previous experimental studies for a single species. Further analysis of the dose-response relationship, especially regarding the interaction effect, will be discussed in Section 4.2.

3.4. Toxicity prediction in the multi-pollutant mixture: FLIT-SHAP vs. Additive model

In multi-pollutant toxicity analysis, isolating the specific contribution of each species to a total toxicity within a given exposure sample is a significant challenge. The SV* shown in Fig. 3, which was the result of FLIT-SHAP, makes the above task possible. Accordingly, we predicted the total and species-specific OPs of real PM samples under multi-pollutant exposure conditions and compared them with those predicted by the additive model, which is based on the dose-response relationship of pure species, as indicated in a previous study [22]. The results are shown in Fig. 4**a** and **b**, respectively. The relative contributions of each species to the total OP for additive and FLIT-SHAP approaches are shown in Fig. 4**c** and **d**, respectively.

The overall OP was lower for all samples and periods in FLIT-SHAP, although some species showed higher OP within samples compared with that of the additive approach; comparison between the additive approach and black box model indicated a same trend (Figs. S9–**11**). Although the variations in concentration are the only method to explain the variation in OP for the additive approach, in FLIT-SHAP, both concentration and multi-pollutant interaction effects are incorporated. First, the concentration effect is evident: for AC* , all quinones exhibited the highest concentrations (Table S1) and OPs (Fig. 4**b**). The highest and lowest concentrations of Fe and Mn corresponded to their highest and lowest OP values, respectively. Second, the interaction effect generally resulted in a decrease in OP, likely owing to antagonistic interactions. In contrast, certain interesting cases are presented as follows: the combined OP caused by all quinones in AC* was higher than that calculated using the additive approach; the lowest Cu concentration (UF) resulted in the highest OP among all cases. The detailed analysis will be discussed in Section 4.3.

The resulting percentage contribution reveals that the additive approach shows little variation, with metals dominating all modes and periods and showing higher contributions during non-haze periods (70–85 %). These trends are consistent with those of previous studies adopting additive assumptions [22; 34]. However, FLIT-SHAP showed more variation across modes and periods, with increased contribution of quinones for some cases, indicating the effect of the multi-pollutant interaction. Further analysis will be discussed in Section 4.3.

4. Discussion

4.1. Novelty of FLIT-SHAP

Current approaches for multi-pollutant toxicity analysis cannot

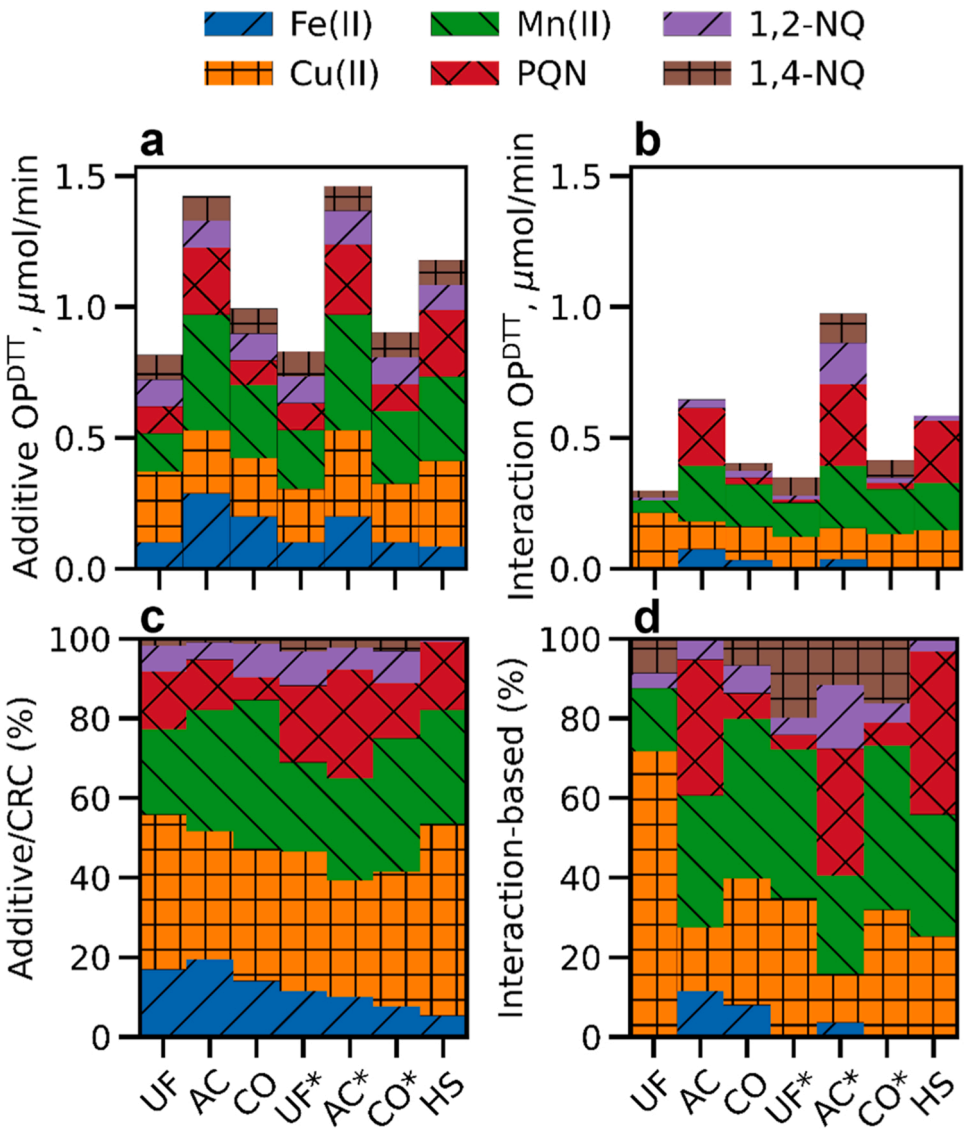

Fig. 4. FLIT-SHAP vs. additive model predictions for real samples. (a) Additive and (b) FLIT-SHAP interaction-based OP. (c) The relative contribution of each species in each sample to the OP based on the concentration-response curve (CRC) of each species in a study conducted by Charrier and Anastasio.[22] (d) The relative contribution of each species is based on (b). UF = ultrafine mode (0.056 μm < d_p < 0.18 μm); AC = accumulation mode (0.18 μm ≤ d_p ≤ 3.2 μm); CO = coarse mode (3.2 μm < d_p < 18 μm); HS = hypothetical $PM_{2.5}$. * Indicates haze periods.

extract information on the dose-response relationship, which limits their application [15]. This is a key motivation for our proposed approach (FLIT-SHAP). The combination of an ML model, such as XGBoost, and FLIT-SHAP enables the (1) determination of the dose-response relationship (overall, main, and interaction); and (2) elucidation of species-specific toxicity in a multi-pollutant mixture, while also considering the interaction effect. Furthermore, we applied our approach to the OP of PM, and this is the first attempt to consider a multi-pollutant mixture in this context as previous studies have only explored binary systems [31–32; 36; 7], which cannot adequately explain the inherently complex PM samples.

4.2. Dose-response pattern of redox-active species in a multi-pollutant mixture

For our case study, the dose-response associations for the main, interaction, and overall effects are shown in Fig. 3. These trends clearly indicate that ME* is only perturbed by changes in concentration and shows little to no dispersion, whereas SV* shows large dispersion and varies with both concentration and IE. Notably, IE also varies with the species type and composition of a sample.

In general, we observed that most IEs were synergistic (55–63 %), followed by antagonistic (25–42 %) and additive (1–15 %), although they varied based on species and concentrations. Considering Fe(II) at concentrations less than 2.5 μM, SV*s are not significantly dispersed above or below the ME*s, implying that they undergo additive interactions within this concentration range. However, as the Fe(II) concentration increases above 2.5 μM, the total interaction becomes synergistic (IE > 0), as reported for Fe-quinone [31,57] (Table S9), and increases with concentration. Cu(II) and Mn(II) exhibited a mix of interactions with higher magnitudes at higher concentrations. Cu(II) predominantly showed synergistic (IE > 0) and antagonistic (IE < 0) interactions at low (<0.5 μM) and high (>0.5 μM) concentrations, respectively, as observed in binary mixtures with 1,2-NQ and PQN [7]. Mn(II) showed a more synergistic interaction (IE > 0) than antagonistic interaction, which is consistent with the results of previous studies (Table S9).

Quinones also exhibited synergistic and antagonistic interactions. To explore the importance of interactions based on the mean values of the absolute pairwise interaction values (Fig. S8), we observed strong

quinone-quinone interactions for the first time in DTT consumption. Fig. S12 shows both synergistic and antagonistic interactions for PQN + 1,2-NQ and 1,2-NQ + 1,4-NQ. As the binary mixture was reported to be additive [31; 7], the presence of other species, such as metals, may affect the interaction between the quinones.

In this study, we considered several species whose interaction effects in binary mixtures have previously been measured [31–32; 36; 7]. These species demonstrated synergistic, antagonistic, and additive effects when mixed with other species, as summarized in Table S9. Although some of these findings aligned with our results, others did not. This discrepancy can be attributed to two factors. First, in most previous studies, the OP of binary mixtures was measured at only one or two concentrations. Second, these studies focused solely on the binary effect. In contrast, in our study, we considered the cumulative multi-pollutant interaction of a species with other species within a sample. Consequently, we anticipate that dominant but opposing interactions will neutralize each other, whereas dominant and similar interactions will amplify each other.

4.3. Application of FLIT-SHAP to OP prediction in real samples

The second advantage of the FLIT-SHAP approach is its ability to distinguish species-specific toxicity in a multi-pollutant mixture. This was achieved by utilizing the obtained dose-response relationship, while also considering the interaction effect. In our case study of OP, we estimated the OP for each redox-active species in the PM samples (Fig. 4). We compared these results with the predictions obtained from the additive model. Overall, we found that the interaction effect led to the underestimation of the total OP by 33–66 %, implying an overall antagonistic effect on the OP (Table S10). We also observed contrasting trends between the additive and FLIT-SHAP predictions (Fig. 4**a** and **b**), which were likely driven by the patterns of multi-pollutant interactions shown in Fig. 3 and **S12.** For instance, the PQN concentrations in AC and UF* were similar, but the OP in AC was approximately 17-fold higher than that in UF* . This discrepancy can be attributed to synergistic interactions resulting from Mn-PQN interactions. When the OP of PQN was high, the concentrations of Mn also tended to be high, ranging from 0.400 to 0.539 mM (Table S1). This observation is consistent with that of a previous study, wherein a synergistic interaction was observed between Mn and PQN when Mn concentrations were high [31].

The higher Cu concentrations in AC, AC* , and HS resulted in lower OP values. This trend is reflected in the Cu-PQN interaction plot (Fig. S12), wherein the Cu contribution shows a negative trend with increasing concentration; this suggests an antagonistic interaction. Notably, the OP of Cu was the highest during UF when its concentration was the lowest. Under this condition, the total concentration and OP of quinones were the lowest, indicating an antagonistic interaction between Cu and quinones. Previous studies have reported such antagonistic interactions in binary mixtures [31; 7] or a simulated $PM_{2.5}$ water extract [38]. The activity of Cu has been attributed to the formation of a metal-organic complex [58,59].

The OP and concentration of 1,2-NQ were the highest in AC* . However, the OP during the other events was significantly low, despite their concentrations not being significantly low. For AC* , the concentration and OP of 1,4-NQ were the highest. Therefore, a synergistic effect may exist between 1,2-NQ and 1,4-NQ, as predicted from Figs. S8 and S12. However, this phenomenon has not been reported in binary mixtures. Notably, although the results in Fig. S12 can be shown for major interacting pairs, each species undergoes multiple interactions, as shown by the IE trends in Fig. 3.

The comparison of the relative contributions of species from the additive and FLIT-SHAP approaches revealed notable trends across different modes and periods (Fig. 4**c** and **d**). In accordance with the results of a previous study [34], FLIT-SHAP revealed that metals generally showed higher contributions during non-haze periods (60–87 %) than during haze periods (40–73 %). However, the contribution of metals was much lower in the accumulation-mode particles, AC, AC* , and HS (40–60 %), whereas quinones contributed up to approximately 60 %, contrary to their contribution according to the additive approach. The higher quinone contribution was mainly driven by PQN, suggesting that the composition of the accumulation-mode particles ($PM_{2.5}$) enhanced the OP of the organic moieties. Additionally, the contribution of 1,4-NQ in FLIT-SHAP was higher than that in the additive model in almost all cases. Some species, such as PQN, 1,4-NQ, and Fe, accounted for zero contribution in some modes, which could be attributed to a net antagonistic interaction, low concentration, or their negligible intrinsic OP compared with those of other species in the multi-pollutant mixture. Overall, the FLIT-SHAP approach (R^2 = 0.99) exhibited notably higher prediction accuracy for the real-world sample OP reported by Lyu et al. [34] compared to the additive model (R^2 = 0.89) as shown in Fig. S13**.** The differences between the measured OP and FLIT-SHAP predictions might arise from (1) the difference in the DTT consumption measurement method employed (Cho method [34] vs Li method [this work]), and (2) the difference in the extraction solvent used for measuring OP and quinone concentrations, respectively (DI water for OP measurement and dichloromethane for quinone concentration measurement [34]). Considering the lower solubility of quinones in water compared to dichloromethane, the lower quinone concentrations in the DTT solution could have resulted in lower OP values than those obtained using the reported concentrations.

While our study enhances the understanding of the OP of PM, it is crucial to acknowledge its limitations. Firstly, considering only a limited set of valence states for metals may be insufficient. Experimental studies have shown that aerosol pH and aging time mediate metal valency and solubility, which in turn affects toxic potency [60]. Furthermore, future research should incorporate the changing valence states of metals with respect to aerosol pH into the training data. This approach will help better understand the interactions, resulting absolute toxicity, and more accurately mimic real-world systems. Secondly, focusing solely on PM restricts the generalization to other exposure mediums. In future studies, the spectrum of species and factors should be broadened, exploring real exposure thresholds for a comprehensive understanding of complex interactions. Additionally, incorporating diverse health effects will provide a more holistic view, aiding the development of effective health risk management strategies and environmental policies.

5. Conclusions

In this study, we introduced FLIT-SHAP, an innovative method to elucidate an individual species effects in a mixture for environmental risk assessment. By localizing the intercept of the SHAP model, FLIT-SHAP estimates individual pollutant effects, providing insights into the dose-response relationships. It highlights limitations in conventional methods, emphasizing the need for accuracy in environmental assessments. When applied to mixtures of multi-redox-active species in PM, FLIT-SHAP can unveil complex interactions influencing the dose-response patterns. Our results emphasize the importance of considering interactions in multi-pollutant exposure analysis. Synergistic effects (55–63 %) suggest potential heightened toxicity based on the sample composition. In contrast, FLIT-SHAP generally indicated lower OP than that obtained by the additive model in real PM samples. Our finding regarding quinones challenges the existing prioritization strategies, paving the way for new research into mixture toxicity mechanisms. The application of FLIT-SHAP marks a significant advancement in understanding the environmental impact of chemical mixtures. Identifying individual pollutant contributions can help the implementation of regulatory decisions more effectively. This approach has immense potential to enhance precision in environmental risk assessment, contributing to informed decision-making for environmental and human health protection. Its nuanced and localized alternative is crucial for accurate environmental risk assessment and policy decisions.

Environmental implication

The studied material, particulate matter (PM), should be considered hazardous because it contains multiple redox-active species that can cause oxidative stress and inflammation in the human body. The work helps address environmental problems by developing a novel method, FLIT-SHAP, that can reveal the individual and interactive effects of these species on the oxidative potential (OP) of PM, which is a measure of its toxicity. FLIT-SHAP can also be applied to other types of chemical mixtures and dose-responses, improving the accuracy and transparency of risk assessment and policy making.

CRediT authorship contribution statement

Charles Esu: Writing – original draft, Methodology, Investigation, Conceptualization. **Kuk Cho:** Writing – review & editing, Validation, Supervision, Conceptualization. **JongCheol Pyo:** Writing – review & editing, Validation.

Declaration of Competing Interest

The authors declare the following financial interests/personal relationships which may be considered as potential competing interests: Kuk Cho reports financial support was provided by National Research Foundation of Korea. If there are other authors, they declare that they have no known competing financial interests or personal relationships that could have appeared to influence the work reported in this paper.

Data availability

Data will be made available on request.

Acknowledgments

This study was supported by the National Research Foundation (NRF) grants funded by the Ministry of Education, Republic of Korea [2020R1A6A1A03044834].

Appendix A. Supporting information

Supplementary data associated with this article can be found in the online version at doi:10.1016/j.jhazmat.2024.134864.

References

[1] Jin, Y., Qi, G., Shou, Y., Li, D., Liu, Y., Guan, H., et al., 2022. High throughput data-based, toxicity pathway-oriented development of a quantitative adverse outcome pathway network linking AHR activation to lung damages. J Hazard Mater 425, 128041. https://doi.org/10.1016/j.jhazmat.2021.128041.

[2] Quiros-Alcala, L., Barr, D.B., 2023. Invited perspective: mixtures—are they worth the risk (Assessment)? Environ Health Perspect 131, 041301. https://doi.org/10.1289/EHP12596.

[3] EPA, U., 2000. Supplementary guidance for conducting health risk assessment of chemical mixtures, EPA, US: Washington, DC, USA.

[4] Backhaus, T., Faust, M., 2012. Predictive environmental risk assessment of chemical mixtures: a conceptual framework. Environ Sci Technol 46, 2564–2573. https://doi.org/10.1021/es2034125.

[5] Laetz, C.A., Baldwin, D.H., Collier, T.K., Hebert, V., Stark, J.D., Scholz, N.L., 2009. The synergistic toxicity of pesticide mixtures: implications for risk assessment and the conservation of endangered pacific salmon. Environ Health Perspect 117, 348–353. https://doi.org/10.1289/ehp.0800096.

[6] Bjergager, M.-B.A., Hanson, M.L., Lissemore, L., Henriquez, N., Solomon, K.R., Cedergreen, N., 2011. Synergy in microcosms with environmentally realistic concentrations of prochloraz and esfenvalerate. Aquat Toxicol 101, 412–422. https://doi.org/10.1016/j.aquatox.2010.11.004.

[7] Yu, H., Wei, J., Cheng, Y., Subedi, K., Verma, V., 2018. Synergistic and antagonistic interactions among the particulate matter components in generating reactive oxygen species based on the dithiothreitol assay. Environ Sci Technol 52, 2261–2270. https://doi.org/10.1021/acs.est.7b04261.

[8] Martin, O., Scholze, M., Ermler, S., McPhie, J., Bopp, S.K., Kienzler, A., et al., 2021. Ten years of research on synergisms and antagonisms in chemical mixtures: a systematic review and quantitative reappraisal of mixture studies. Environ Int 146, 106206. https://doi.org/10.1016/j.envint.2020.106206.

[9] Wu, X., Zhou, Q., Mu, L., Hu, X., 2022. Machine learning in the identification, prediction and exploration of environmental toxicology: challenges and perspectives. J Hazard Mater 438, 129487. https://doi.org/10.1016/j.jhazmat.2022.129487.

[10] Bobb, J.F., Valeri, L., Claus Henn, B., Christiani, D.C., Wright, R.O., Mazumdar, M., et al., 2015. Bayesian kernel machine regression for estimating the health effects of multi-pollutant mixtures. Biostatistics 16, 493–508. https://doi.org/10.1093/biostatistics/kxu058.

[11] Carrico, C., Gennings, C., Wheeler, D.C., Factor-Litvak, P., 2015. Characterization of weighted quantile sum regression for highly correlated data in a risk analysis setting. J Agric, Biol, Environ Stat 20, 100–120. https://doi.org/10.1007/s13253-014-0180-3.

[12] Keil, A.P., Buckley, J.P., O'Brien, K.M., Ferguson, K.K., Zhao, S., White, A.J., 2020. A quantile-based g-computation approach to addressing the effects of exposure mixtures. Environ Health Perspect 128, 047004. https://doi.org/10.1289/EHP5838.

[13] Li, Y.-C., Hsu, H.-H.L., Chun, Y., Chiu, P.-H., Arditi, Z., Claudio, L., et al., 2021. Machine learning–driven identification of early-life air toxic combinations associated with childhood asthma outcomes. J Clin Investig 131. https://doi.org/10.1172/jci152088.

[14] Midya, V., Alcala, C.S., Rechtman, E., Gregory, J.K., Kannan, K., Hertz-Picciotto, I., et al., 2023. Machine learning assisted discovery of interactions between pesticides, phthalates, phenols, and trace elements in child neurodevelopment. Environ Sci Technol 57, 18139–18150. https://doi.org/10.1021/acs.est.3c00848.

[15] Savitz, D.A., Hattersley, A.M., 2023. Evaluating chemical mixtures in epidemiological studies to inform regulatory decisions. Environ Health Perspect 131, 045001. https://doi.org/10.1289/EHP11899.

[16] Lundberg, S.M., Erion, G., Chen, H., Degrave, A., Prutkin, J.M., Nair, B., et al., 2020. From local explanations to global understanding with explainable AI for trees. Nat Mach Intell 2, 56–67. https://doi.org/10.1038/s42256-019-0138-9.

[17] Lundberg, S.M., Nair, B., Vavilala, M.S., Horibe, M., Eisses, M.J., Adams, T., et al., 2018. Explainable machine-learning predictions for the prevention of hypoxaemia during surgery. Nat Biomed Eng 2, 749–760. https://doi.org/10.1038/s41551-018-0304-0.

[18] Bates, J.T., Fang, T., Verma, V., Zeng, L., Weber, R.J., Tolbert, P.E., et al., 2019. Review of acellular assays of ambient particulate matter oxidative potential: methods and relationships with composition, sources, and health effects. Environ Sci Technol 53, 4003–4019. https://doi.org/10.1021/acs.est.8b03430.

[19] Abrams, J.Y., Weber, R.J., Klein, M., Samat, S.E., Chang, H.H., Strickland, M.J., et al., 2017. Associations between ambient fine particulate oxidative potential and cardiorespiratory emergency department visits. Environ Health Perspect 125, 107008. https://doi.org/10.1289/ehp1545.

[20] Antiñolo, M., Willis, M.D., Zhou, S., Abbatt, J.P.D., 2015. Connecting the oxidation of soot to its redox cycling abilities. Nat Commun 6, 6812. https://doi.org/10.1038/ncomms7812.

[21] Calas, A., Uzu, G., Kelly, F.J., Houdier, S., Martins, J.M.F., Thomas, F., et al., 2018. Comparison between five acellular oxidative potential measurement assays performed with detailed chemistry on PM10 samples from the city of Chamonix (France). Atmos Chem Phys 18, 7863–7875. https://doi.org/10.5194/acp-18-7863-2018.

[22] Charrier, J.G., Anastasio, C., 2012. On dithiothreitol (DTT) as a measure of oxidative potential for ambient particles: evidence for the importance of soluble transition metals. Atmos Chem Phys 12, 9321–9333. https://doi.org/10.5194/acp-12-9321-2012.

[23] Charrier, J.G., Richards-Henderson, N.K., Bein, K.J., McFall, A.S., Wexler, A.S., Anastasio, C., 2015. Oxidant production from source-oriented particulate matter – Part 1: Oxidative potential using the dithiothreitol (DTT) assay. Atmos Chem Phys 15, 2327–2340. https://doi.org/10.5194/acp-15-2327-2015.

[24] Cheng, Y., Ma, Y., Dong, B., Qiu, X., Hu, D., 2021. Pollutants from primary sources dominate the oxidative potential of water-soluble PM2.5 in Hong Kong in terms of dithiothreitol (DTT) consumption and hydroxyl radical production. J Hazard Mater 405, 124218. https://doi.org/10.1016/j.jhazmat.2020.124218.

[25] Cheung, K., Shafer, M.M., Schauer, J.J., Sioutas, C., 2012. Diurnal trends in oxidative potential of coarse particulate matter in the los angeles basin and their relation to sources and chemical composition. Environ Sci Technol 46, 3779–3787. https://doi.org/10.1021/es204211v.

[26] Cho, A.K., Sioutas, C., Miguel, A.H., Kumagai, Y., Schmitz, D.A., Singh, M., et al., 2005. Redox activity of airborne particulate matter at different sites in the Los Angeles Basin. Environ Res 99, 40–47. https://doi.org/10.1016/j.envres.2005.01.003.

[27] Daellenbach, K.R., Uzu, G., Jiang, J., Cassagnes, L.-E., Leni, Z., Vlachou, A., et al., 2020. Sources of particulate-matter air pollution and its oxidative potential in Europe. Nature 587, 414–419. https://doi.org/10.1038/s41586-020-2902-8.

[28] Daher, N., Saliba, N.A., Shihadeh, A.L., Jaafar, M., Baalbaki, R., Shafer, M.M., et al., 2014. Oxidative potential and chemical speciation of size-resolved particulate matter (PM) at near-freeway and urban background sites in the greater Beirut area. Sci Total Environ 470-471, 417–426. https://doi.org/10.1016/j.scitotenv.2013.09.104.

[29] Dou, J., Lin, P., Kuang, B.-Y., Yu, J.Z., 2015. Reactive oxygen species production mediated by humic-like substances in atmospheric aerosols: enhancement effects by pyridine, imidazole, and their derivatives. Environ Sci Technol 49, 6457–6465. https://doi.org/10.1021/es5059378.

[30] Fang, T., Zeng, L., Gao, D., Verma, V., Stefaniak, A.B., Weber, R.J., 2017. Ambient size distributions and lung deposition of aerosol dithiothreitol-measured oxidative

potential: contrast between soluble and insoluble particles. Environ Sci Technol 51, 6802–6811. https://doi.org/10.1021/acs.est.7b01536.
[31] Guo, H., Fu, H., Jin, L., Huang, S., Li, X., 2020. Quantification of synergistic, additive and antagonistic effects of aerosol components on total oxidative potential. Chemosphere 252, 126573. https://doi.org/10.1016/j.chemosphere.2020.126573.
[32] Lin, M., Yu, J.Z., 2019. Effect of metal-organic interactions on the oxidative potential of mixtures of atmospheric humic-like substances and copper/manganese as investigated by the dithiothreitol assay. Sci Total Environ 697, 134012. https://doi.org/10.1016/j.scitotenv.2019.134012.
[33] Liu, Q., Baumgartner, J., Zhang, Y., Liu, Y., Sun, Y., Zhang, M., 2014. Oxidative potential and inflammatory impacts of source apportioned ambient air pollution in Beijing. Environ Sci Technol 48, 12920–12929. https://doi.org/10.1021/es5029876.
[34] Lyu, Y., Guo, H., Cheng, T., Li, X., 2018. Particle size distributions of oxidative potential of lung-deposited particles: assessing contributions from quinones and water-soluble metals. Environ Sci Technol 52, 6592–6600. https://doi.org/10.1021/acs.est.7b06686.
[35] Verma, V., Fang, T., Xu, L., Peltier, R.E., Russell, A.G., Ng, N.L., et al., 2015. Organic aerosols associated with the generation of reactive oxygen species (ROS) by water-soluble $PM_{2.5}$. Environ Sci Technol 49, 4646–4656. https://doi.org/10.1021/es505577w.
[36] Wang, S., Ye, J., Soong, R., Wu, B., Yu, L., Simpson, A.J., et al., 2018. Relationship between chemical composition and oxidative potential of secondary organic aerosol from polycyclic aromatic hydrocarbons. Atmos Chem Phys 18, 3987–4003. https://doi.org/10.5194/acp-18-3987-2018.
[37] Xiong, Q., Yu, H., Wang, R., Wei, J., Verma, V., 2017. Rethinking dithiothreitol-based particulate matter oxidative potential: measuring dithiothreitol consumption versus reactive oxygen species generation. Environ Sci Technol 51, 6507–6514. https://doi.org/10.1021/acs.est.7b01272.
[38] Yu, Q., Chen, J., Qin, W., Ahmad, M., Zhang, Y., Sun, Y., et al., 2022. Oxidative potential associated with water-soluble components of PM2.5 in Beijing: the important role of anthropogenic organic aerosols. J Hazard Mater 433, 128839. https://doi.org/10.1016/j.jhazmat.2022.128839.
[39] Chen, T., Guestrin, C., XGBoost: A Scalable Tree Boosting System, in: Proceedings of the 22nd ACM SIGKDD International Conference on Knowledge Discovery and Data Mining, Association for Computing Machinery, San Francisco, California, USA, 2016, pp. 785–794.
[40] Majestic, B.J., Schauer, J.J., Shafer, M.M., 2007. Application of synchrotron radiation for measurement of iron red-ox speciation in atmospherically processed aerosols. Atmos Chem Phys 7, 2475–2487. https://doi.org/10.5194/acp-7-2475-2007.
[41] Alam, M.S., Delgado-Saborit, J.M., Stark, C., Harrison, R.M., 2013. Using atmospheric measurements of PAH and quinone compounds at roadside and urban background sites to assess sources and reactivity. Atmos Environ 77, 24–35. https://doi.org/10.1016/j.atmosenv.2013.04.068.
[42] Charrier, J.G., Anastasio, C., 2015. Rates of hydroxyl radical production from transition metals and quinones in a surrogate lung fluid. Environ Sci Technol 49, 9317–9325. https://doi.org/10.1021/acs.est.5b01606.
[43] Cho, A.K., Di Stefano, E., You, Y., Rodriguez, C.E., Schmitz, D.A., Kumagai, Y., et al., 2004. Determination of four quinones in diesel exhaust particles, SRM 1649a, and atmospheric $PM_{2.5}$. special issue of aerosol science and technology on findings from the fine particulate matter supersites program. Aerosol Sci Technol 38, 68–81. https://doi.org/10.1080/02786820390229471.
[44] Chung, M.Y., Lazaro, R.A., Lim, D., Jackson, J., Lyon, J., Rendulic, D., et al., 2006. Aerosol-borne quinones and reactive oxygen species generation by particulate matter extracts. Environ Sci Technol 40, 4880–4886. https://doi.org/10.1021/es0515957.
[45] Eiguren-Fernandez, A., Miguel, A.H., Di Stefano, E., Schmitz, D.A., Cho, A.K., Thurairatnam, S., et al., 2008. Atmospheric distribution of gas- and particle-phase quinones in Southern California. Aerosol Sci Technol 42, 854–861. https://doi.org/10.1080/02786820802339546.
[46] Li, Q., Wyatt, A., Kamens, R.M., 2009. Oxidant generation and toxicity enhancement of aged-diesel exhaust. Atmos Environ 43, 1037–1042. https://doi.org/10.1016/j.atmosenv.2008.11.018.
[47] Lin, M., Yu, J.Z., 2019. Dithiothreitol (DTT) concentration effect and its implications on the applicability of DTT assay to evaluate the oxidative potential of atmospheric aerosol samples. Environ Pollut 251, 938–944. https://doi.org/10.1016/j.envpol.2019.05.074.
[48] Fang, T., Verma, V., Guo, H., King, L.E., Edgerton, E.S., Weber, R.J., 2015. A semi-automated system for quantifying the oxidative potential of ambient particles in aqueous extracts using the dithiothreitol (DTT) assay: results from the Southeastern Center for Air Pollution and Epidemiology (SCAPE). Atmos Meas Tech 8, 471–482. https://doi.org/10.5194/amt-8-471-2015.
[49] Gao, D., Fang, T., Verma, V., Zeng, L., Weber, R.J., 2017. A method for measuring total aerosol oxidative potential (OP) with the dithiothreitol (DTT) assay and comparisons between an urban and roadside site of water-soluble and total OP. Atmos Meas Tech 10, 2821–2835. https://doi.org/10.5194/amt-10-2821-2017.
[50] Wu, J., Yang, C., Zhang, C., Cao, F., Wu, A., Zhang, Y., 2022. Development, characterization, and application of an improved online reactive oxygen species analyzer based on the Monitor for AeRosols and Gases in ambient Air (MARGA). Atmos Meas Tech 15, 2623–2633. https://doi.org/10.5194/amt-15-2623-2022.
[51] Shi, Z., Song, C., Liu, B., Lu, G., Xu, J., Van Vu, T., et al., 2021. Abrupt but smaller than expected changes in surface air quality attributable to COVID-19 lockdowns. Sci Adv 7, eabd6696. https://doi.org/10.1126/sciadv.abd6696.
[52] Song, C., Becagli, S., Beddows, D.C.S., Brean, J., Browse, J., Dai, Q., et al., 2022. Understanding sources and drivers of size-resolved aerosol in the high arctic islands of svalbard using a receptor model coupled with machine learning. Environ Sci Technol 56, 11189–11198. https://doi.org/10.1021/acs.est.1c07796.
[53] Zhong, S., Zhang, K., Wang, D., Zhang, H., 2021. Shedding light on “Black Box” machine learning models for predicting the reactivity of HO radicals toward organic compounds. Chem Eng J 405, 126627. https://doi.org/10.1016/j.cej.2020.126627.
[54] Lundberg, S.M., Lee, S.-I., 2017. A unified approach to interpreting model predictions. Proceedings of the 31st International Conference on Neural Information Processing Systems. Curran Associates Inc,, Long Beach, California, USA, pp. 4768–4777.
[55] Pedregosa, F., Varoquaux, G., Gramfort, A., Michel, V., Thirion, B., Grisel, O., et al., 2011. Scikit-learn: machine learning in python. J Mach Learn Res 12, 2825–2830.
[56] Delgado-Saborit, J.M., Alam, M.S., Godri Pollitt, K.J., Stark, C., Harrison, R.M., 2013. Analysis of atmospheric concentrations of quinones and polycyclic aromatic hydrocarbons in vapour and particulate phases. Atmos Environ 77, 974–982. https://doi.org/10.1016/j.atmosenv.2013.05.080.
[57] Pietrogrande, M.C., Romanato, L., Russo, M., 2022. Synergistic and antagonistic effects of aerosol components on its oxidative potential as predictor of particle toxicity. Toxics 10, 196.
[58] Kachur, A.V., Held, K.D., Koch, C.J., Biaglow, J.E., 1997. Mechanism of production of hydroxyl radicals in the copper-catalyzed oxidation of dithiothreitol. Radiat Res 147, 409–415. https://doi.org/10.2307/3579496.
[59] Wei, J., Yu, H., Wang, Y., Verma, V., 2019. Complexation of iron and copper in ambient particulate matter and its effect on the oxidative potential measured in a surrogate lung fluid. Environ Sci Technol 53, 1661–1671. https://doi.org/10.1021/acs.est.8b05731.
[60] Song, X., Wu, D., Chen, X., Ma, Z., Li, Q., Chen, J., 2024. Toxic potencies of particulate matter from typical industrial plants mediated with acidity via metal dissolution. Environ Sci Technol 58, 6736–6743. https://doi.org/10.1021/acs.est.4c00929.